GPS Solut (2014) 18:231–242
DOI 10.1007/s10291-013-0324-x

ORIGINAL ARTICLE

Using Allan variance to analyze the error characteristics of GNSS positioning

Xiaoji Niu · Qijin Chen · Quan Zhang · Hongping Zhang · Jieming Niu · Kejie Chen · Chuang Shi · Jingnan Liu

Received: 5 August 2012 / Accepted: 24 March 2013 / Published online: 17 April 2013

Abstract Currently, we evaluate the positioning accuracy of GNSS mainly by providing statistical values that can represent the overall error level, such as CEP, RMS, 2DRMS, and maximum error. These are solid indicators of the general performance of the GNSS positioning. But some applications like GNSS/INS integrated system require a detailed analysis of the error characteristics and knowledge of the precise error model. This requirement necessitates the modeling of the error components of the GNSS positioning solutions. In our research, the Allan variance method is proposed to analyze the GNSS positioning errors, describe the error characteristics, and build the corresponding error models. Based on our research, four dominant noise terms are identified in the GNSS positioning solutions, that is, 1st order Gauss-Markov process, Gaussian white noise, random walk noise, and flicker noise, which indicates that white noise is not always enough and appropriate to model GNSS positioning errors for some applications. The results show that the Allan variance is a feasible and effective way to analyze the error characteristics of the GNSS positioning solutions.

Keywords GNSS positioning · Allan variance · Error analysis · Error modeling · Time series

X. Niu · Q. Zhang · H. Zhang · K. Chen · C. Shi (✉) · J. Liu
GNSS Research Center, Wuhan University, No.129, Luoyu Road, Wuhan, Hubei 430079, People's Republic of China
e-mail: shi@whu.edu.cn

Q. Chen · J. Niu
School of Geodesy and Geomatics, Wuhan University, No.129, Luoyu Road, Wuhan, Hubei 430079, People's Republic of China

Introduction

Global Navigation Satellite System (GNSS) has been applied in almost every field, where position information is needed, such as GNSS-aided INS (inertial navigation system). For GNSS/INS loosely coupled integrated system, the GPS position is used to estimate the errors in the INS state and calibrate the inertial sensor. The GNSS/INS integration algorithm normally uses Kalman filter to fuse data. The standard Kalman filter requires the measurement noise to be white noise. Most of the algorithm designs regard GNSS error as white noise to make it simple to handle (Shin 2001; Groves 2008). However, treating all of them as white noise will cause the Kalman filter output variance/covariance matrix, that is, P matrix, to be smaller than the realistic estimation error level, that is, too optimistic. Therefore, some researchers suggest enlarging the parameter of the GNSS white noise in the Kalman filter, that is, the measurement error variance matrix of Kalman filter, that is, R matrix, to somehow compensate the inconsistency issue (Groves 2008). But this method is just a compromise. Actually, almost all of the GNSS-related error sources are time or space correlated, such as ephemeris errors, ionospheric and tropospheric delay, and satellite geometry (Tralli and Lichten 1990; Rankin 1994; Bierman 1995; Ge and Liu 1996). We speculate white noise is not always optimal for modeling the GNSS positioning error in some applications.

A number of pioneering studies investigated the error characteristics related to GNSS position solutions, which can be classified into two categories roughly. Some focused on investigating and modeling the GNSS error sources, such as troposphere delay (Rankin 1994; Bierman 1995; Ge and Liu 1996) and receiver clock error. Others focused on the coordinate instability of the monitoring station derived

by GNSS position (King et al. 1995; Langbein and Johnson 1997; Zhang et al. 1997; Mao et al. 1999; Bock et al. 2000; Williams et al. 2004; Amiri-Simkooei et al. 2007; Khelifa et al. 2011). However, to the authors' knowledge, few attempts have been made to investigate the positioning error of GNSS technique itself.

For the previous works related to the GNSS positioning error analysis, Friederichs (2010) made an attempt to describe the applications of the Allan variance in the geodetic time series analysis including the GPS positioning errors, but he did not analyze the error characteristics in details, and the precise error model in GPS positioning error had not been given in his research. Some references can be found to analyze the temporal correlation property of the GPS positioning error or GPS baseline time series to investigate time correlation property of the observations and the measurement noise of GPS receivers (Howind et al. 1999; Borre and Tiberius 2000; El-Rabbany and Kleusberg 2003; Amiri-Simkooei et al. 2007). Bock et al. (2000) proposed the instantaneous GPS positioning method and studied the characteristics of the geodetic positioning at medium distances. Genrich and Bock (2006) analyzed spectral characteristics of 10–50 Hz instantaneous relative positions over short- and medium-scale GPS baselines. Although their research interest is different from what we focus on, these previous works greatly inspired our research. The innovation in our research lies in the fact that it characterizes the errors in GPS positioning solutions.

The Allan variance method is a typical time-based domain analysis technique. Applications of the Allan variance have been extended to geodetic data analysis (Feissel-Vernier et al. 2007; Friederichs 2010; Malkin 2011; Hackl et al. 2011). For instance, the Allan variance method was applied to identify the temporal upper limit accuracy of GPS-based monitoring system (Roberts et al. 2002). Khelifa et al. (2011) applied Allan variance method to identify the noise type of the weekly time series of GPS station coordinate residuals. We also propose to use this method, that is, Allan variance analysis method to analyze the error characteristics of the GNSS positioning solutions.

Our study differs from previous research in the following two aspects. First, we focus on analyzing the characteristics of GNSS positioning error itself rather than the geodetic coordinates or the motion of the station derived from GNSS. Second, the Allan variance method is not only applied to identify the noise types, but also to estimate their coefficients. Precise models of the GNSS positioning errors have been built which is instructive for investigating the GNSS positioning error sources.

Methodology

Allan variance is a time-based domain analysis technique originally developed to study the frequency stability of precision oscillators. It has become a popular method to characterize the errors of inertial sensor. The Allan variance analysis has been widely used and accepted as a preferred method for identifying stochastic processes, such as quantization noise, white noise, correlated noise, sinusoidal noise, random walk, and flicker noise.

Allan variance analysis method

The definition and explanation of the Allan variance method can be found in IEEE (2008a) for detail. The analysis procedure can be described as follow (Niu et al. 2010).

(a) Divide the entire dataset into certain clusters, with a cluster length of T or cluster time T.
(b) Calculate the mean value of each cluster.
(c) Calculate the difference on the mean values of every two successive clusters.
(d) Calculate the mean square of these differences and divide by two. This value is called the Allan variance (σ^2) corresponding to the cluster time T, which represents the signal instability on the time scale of T.
(e) Change the cluster time T from small to large and calculate the Allan variances, so as to scan the signal instability on different time scales.
(f) Draw the log–log plot of the Allan deviation, that is, square root of the Allan variance versus the cluster time T, which is called Allan variance plot, to analyze the error characteristics.

The mathematic form of the Allan variance is:

$$\sigma^2(T) = \frac{1}{2(N_C - 1)} \sum_{k=1}^{N_C - 1} (\bar{y}_{k+1} - \bar{y}_k)^2 \quad (1)$$

where $\bar{y}_k$ is the mean value of the cluster, N_C is the total number of the clusters, σ^2 is the Allan variance, and T is the cluster time/length.

If different spectral noise components are assumed to be described by different power spectral density (PSD) laws, then examination of a log–log plot of Allan deviation versus cluster time allows different noise types to be distinguished by the slope of the plot in particular time regions and the magnitudes of these noise components to be determined (Land et al. 2007). As indicated in IEEE (2008b), the Allan variance analysis can be used for model identification and parameter estimation. Figure 1 is a typical Allan deviation plot with different noise types.

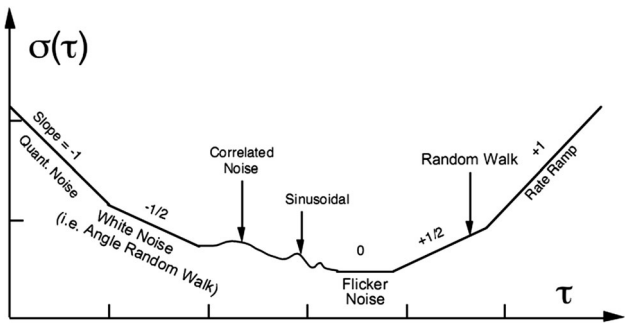

Fig. 1 Sample plot of Allan variance analysis results (IEEE 2008a)

Estimation accuracy of Allan variance

Estimation accuracy of the Allan variance for a specific cluster length T, or cluster time T, depends on the number of independent clusters within the dataset. From a dataset with finite length a finite number of clusters can be generated. The percentage error δ in estimating $\sigma(m)$ when using clusters containing m data points from a dataset of M points is given by:

$$\delta(m) = \frac{1}{\sqrt{2(\frac{M}{m} - 1)}} \tag{2}$$

Equation (2) shows that the estimation errors in the regions of short/long cluster length are small/large as the number of independent clusters in these regions is large/small. EI-Sheimy et al. (2008) gave an example to demonstrate this equation. If there are 2000 data points and the cluster sizes of 500 points are used, the percentage error in estimating $\sigma(T)$ is approximately 40 %. On the other hand, for the short cluster containing ten points, the percentage error is about 5 %. It must be noted that in case the total data points of the raw dataset is too small, for example, only 10 data points, it is not possible to get a set of Allan variance values that are statistically significant and form an Allan plot with sufficient accuracy. Here, we calculate the Allan variance in the form of fully overlapping Allan deviation for greater confidence (Riley 2008).

Noise models

Four types of stochastic processes of particular interest for GNSS positioning solutions are listed below. The related physical phenomena and sources will be explained in the result and analysis section.

(a) Gaussian white noise: On the Allan deviation log–log plot, this noise type is characterized by a region of −1/2 slope, whereas in PSD log–log plot with a region of 0 slope IEEE (2008a).
(b) Flicker noise: On the Allan deviation log–log plot this noise type is shown as a region of 0 slope, but is indicated with a -1 slope in PSD log–log plots IEEE (2008b).
(c) Random walk: This type of noise is associated with an Allan deviation log–log plot with a region of +1/2 slope; and with a region of -2 slope for PSD log–log plot IEEE (2008a).
(d) 1st order Gauss-Markov (GM) process, namely exponentially correlated noise. The details are listed in Table 1

Test setup and GNSS data processing

We analyzed GNSS positioning solutions in three different modes, including post-processing carrier phase differential GPS (DGPS), precise point positioning (PPP), and single point positioning (SPP) at 1 and 50 Hz data rates. We collected multiple datasets using Trimble NetR8 and Trimble NetR9 receivers. Two kinds of experiments were conducted consisting of six static datasets for each: one with length of 24 h at 1 Hz and one with length of 2 h at 50 Hz where both dual-frequency carrier phase and pseudorange were recorded. The Trimble NetR8 receiver is located at Wuhan University IGS reference station. The Trimble NetR9 receiver is positioned at WHUC with known coordinates on the rooftop of the GNSS Research Center at Wuhan University as shown in Fig. 2. To minimize the multipath effects, the following measures are applied: (a) GPS antennas of good quality are used as illustrated in Table 2;

Table 1 Features of Allan variance plots for typical noise terms

Noise type	Allan variance	Coefficient	Curve slope	Coefficient value
White noise	$\frac{N^2}{T}$	N	$-1/2$	$N = \sigma(1)$
Flicker noise	$\frac{2B^2 \ln 2}{\pi}$	B	0	$B = \sigma(f_0)$
Random walk	$\frac{K^2 T}{3}$	K	$+1/2$	$K = \sigma(3)$
GM process	$\sigma^2(T) = \frac{(q_c T_c)^2}{T}\left[1 - \frac{T_c}{2T}\left(3 - 4e^{-\frac{T}{T_c}} + e^{-\frac{2T}{T_c}}\right)\right]$	T_C, σ_{GM}	$\pm 1/2$	$T_c = \frac{T_{\max}}{1.89}, \sigma_{GM} = \sqrt{0.5 q_c T_c}$

Fig. 2 Antenna connected to Trimble NetR9 receiver located on the rooftop of the GNSS Research Center at Wuhan University

(b) Both GPS antennas are set in fairly favorable circumstance where the reflective signal can be negligible; (c) The observations of satellites with elevations angle below 10 ° are rejected in the GNSS data processing.

The datasets at 1 Hz and length of 12–24 h were processed to analyze the long-term low-frequency noise characteristics, whereas datasets at 50 Hz and relatively short-time length of 1–2 h were processed for analyzing the short-term high-frequency noise components. Since processing long-time datasets at 50 Hz needs significant computer resources and it is actually not necessary to process long-time high-rate data, the 1 Hz data were selected as long-time datasets. The datasets involved in the analysis were collected in static mode, because: (a) the static datasets are capable of reflecting most GPS error sources except the effect of multipath, which is complex and varies in different environment; (b) the long-time kinematic datasets are not feasible to be collected and the qualified positioning truth for kinematic epochs is hard to be obtained. For the DGPS analysis, the smoothed DGPS positioning solutions are of high accuracy, for example, 2 cm (1σ) in horizontal, so the accuracy of the reference truth should be one order of magnitude higher, namely millimeter accuracy, which is difficult to acquire in kinematic circumstance. We processed the static dataset in kinematic modes in our research. In such case, accurate reference value is available and the GPS position error series can be easily computed. The following sections describe in detail the data acquisition and the data processing strategy.

Datasets for DGPS solution

The datasets collected at the IGS station were used as the master and those collected by Trimble NetR9 at the roof of the GNSS Research Center were used as the rover. The datasets were processed with GrafNav software v.8.30 developed by Waypoint Group at NovAtel Inc. (http://www.novatel.com) in post-processing kinematic mode. The length of the baseline between the master and the rover is about 500 m.

Datasets for PPP solution

The datasets were processed with the PANDA (**P**ositioning **A**nd **N**avigation **D**ata **A**nalyst) software (Liu and Ge 2003) developed at Wuhan University, in post-processing kinematic mode. Precise IGS final orbit and satellite clock files at 30-s interval were used in the data processing. In addition, corrections for geophysical effects, such as pole and ocean tide effects, have been applied.

Datasets for SPP solution

The datasets for SPP solution were processed with RTKLIB program package v. 2.4.1 (http://www.rtklib.com) in "Single" mode. The dual-frequency observations were used for ionospheric correction, and the "Saastamoinen" model was used for tropospheric correction. Even though the Saastamoinen model is old, the differences of tropospheric correction by different models are small compared to the overall SPP positioning error.

Table 2 lists additional details of the datasets including the length, the antenna type, and the solution types. The positioning error series were calculated using the precisely known coordinates of the stations WUHN and WHUC, then the positioning error at each epoch were transformed to local level coordinates.

Table 2 Dataset collections and GNSS processing

Positioning mode	Data rate (Hz)	Data length (h)	Receiver and antenna	Processing software	Solution
DGPS	1	24	Trimble NetR8 and NetR9	GrafNav 8.30	Kinematic and smoothing
	50	2	Dorne Margolin with choke ring		
PPP	1	12	Trimble NetR9	PANDA	Kinematic and smoothing
	50	1.25	Zephyr GNSS Geodetic II		
SPP	1	24	Trimble NetR9	RTKLIB	Single and Combined
			Zephyr GNSS Geodetic II	2.4.1	

The Allan variance method is applied to the time series of positioning error along the east, north, and up directions to obtain the Allan plots. Then, error models and their parameters were estimated from the Allan plots. Six groups of GPS solutions in DGPS mode were discussed to illustrate the repeatability of the results. Additionally, the PSD method was applied to the same datasets to validate the result from the Allan variance method is reasonable.

Results and analysis

In this section, we will discuss the post-processing DGPS solutions in great details as an example to illustrate the Allan variance analysis method for analyzing GNSS positioning error characteristics. The analysis for PPP and SPP solutions are similar to that of DGPS, so their results will be presented without detailed discussion.

Allan variance analysis to DGPS solution

DGPS solutions of 1 and 50 Hz will be analyzed by the Allan variance analysis method for characterizing the positioning error. The error sources will be discussed in details.

DGPS solution of 1 Hz

Figure 3 shows the time series of the positioning error of DGPS solution at 1 Hz in the east, north, and up directions, which indicates the post-processing kinematic DGPS can reach the precision of 4 mm and 10 mm (1σ) in horizontal and vertical directions, respectively. Such statistic summary parameters, that is, 1σ, can indicate the overall accuracy of the GNSS positioning in a concise way, but it cannot reflect the details of the error characteristics. This figure shows that dU is noisier than dE and dN as generally expected. By applying the Allan variance analysis method to the entire dataset along these three directions, we can obtain the log–log plots of Allan deviation versus cluster time as shown in Fig. 4.

Figure 4 shows that the Allan deviation curves in the east, north, and up directions are of similar shape, with the magnitude of the vertical component apparently greater than that of the horizontal. As discussed before, this is because GPS provides better positioning accuracy in horizontal directions.

The vertical component of the Allan plot in Fig. 4 will be used as an example to illustrate how to identify noise type and to estimate their coefficients. A dashed straight line with a slope of -0.41, which is close to $-1/2$, fits the beginning part of the curve and crosses $T = 1$ s at a value of 3.9 mm. This means that white noise with strength of 3.9

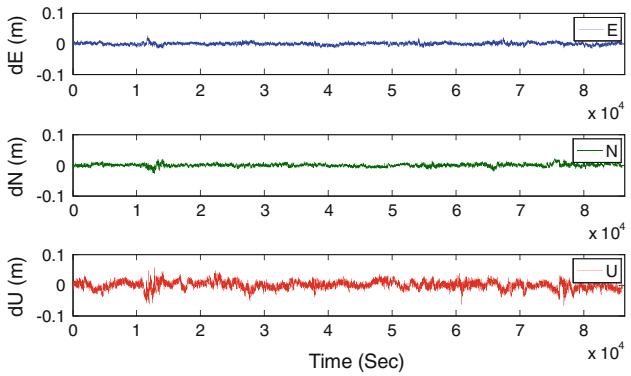

Fig. 3 Positioning error of DGPS solution (1 Hz)

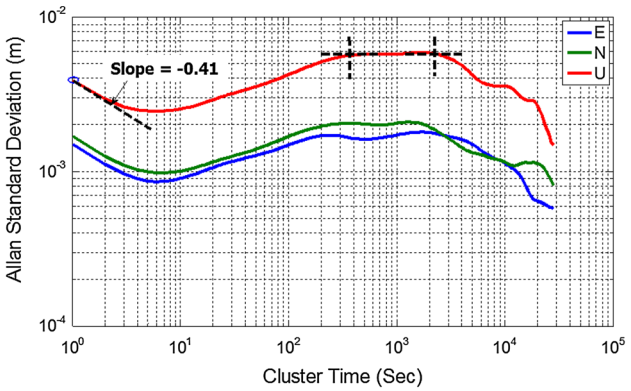

Fig. 4 Allan plots of DGPS solution (1 Hz)

$mm/\sqrt{Hz}$ is the dominant noise term for the short cluster time below 10 s. The time series of DGPS position errors contains 86,400 (i.e., 3,600*24) data points and the coefficient for white noise is estimated at cluster time $T = 1$ s; therefore, the number of independent clusters is 86,400, resulting in an estimation percentage error of smaller than 1/sqrt(2*(86,400−1)) = 0.24 %. The difference in white noise part's slope of -0.41 and $-1/2$ may be explained by influence of adjacent longer-term errors on the right side of the curve. This will be described below.

The white noise portion is followed by two raised points, marked by dashed crosses, in the large cluster time region of $T > 100$ s. This means that the 1st order Gauss-Markov process is the dominant noise in that time region. With these values we can calculate the correlation time and the mean square value of the 1st order Gauss-Markov process as illustrated in Table 1. Table 3 lists the coefficients of noises identified in DGPS solutions at 1 Hz.

For the short-length baseline of 500 m, the main GNSS error sources such as satellite clock drift, ephemeris errors, and propagation delays can be corrected by double difference. Due to the fairly favorable circumstance and the use of choke ring antenna, the multipath disturbance is negligible too. However, the receiver measuring noise and the

Table 3 Noises identified in DGPS solution (1 Hz)

Direction	GM1		GM2		White noise
	T_C (s)	σ_{GM} (mm)	T_C (s)	σ_{GM} (mm)	$N\,(m/\sqrt{Hz})$
E	124.7 ± 4.6	2.8 ± 0.1	920 ± 90	2.9 ± 0.9	1.5
N	130.5 ± 5.0	3.3 ± 0.1	840 ± 80	3.3 ± 0.3	1.7
U	175.4 ± 7.7	9.1 ± 0.4	1,240 ± 150	9.3 ± 1.1	3.9

residual tropospheric delay cannot be eliminated completely, which would therefore remain as the dominant error sources.

The white noise identified in the small cluster time region is most likely induced by the receiver measurement noise. This is because (a) the residual tropospheric delay would most likely cause long-term time-correlated noise in the DGPS solutions; (b) the GPS receiver noise at sampling rate below 1 Hz can be regarded as independent without any time correlation (Borre and Tiberius 2000). For large cluster time region, for example, above 100 s, the dominant noise terms show time-correlated properties. Two aspects may cause time correlation in GPS positioning time series. One is that the observations are noisy so that some signal smoothing or filtering has been applied to reduce the noise level. The other is that some time correlation error sources, such as multipath and atmospheric delays, remain in the time series after data processing (Amiri-Simkooei et al. 2007). So the most possible cause of this time-correlated noise term is the remaining tropospheric delay (Howind et al. 1999), which is difficult to be eliminated completely especially for the wet component (Tralli and Lichten 1990; Ge and Liu 1996). The tropospheric path delay shows time-correlated property, which can be modeled as 1st Gauss-Markov process (Rankin 1994; Ge and Liu 1996).

In the following, two strategies are applied to validate the rationality of the error models analyzed based on Allan plots: a) if the noise components can be reconstructed with the coefficients listed in Table 3 and one obtains the same Allan plots, the rationality of the analysis above can be validated. b) Checking whether the Allan results are consistent with that of conventional time series analysis method PSD. We use MATLAB to simulate an error time series consisting of white noise and 1st order Gauss-Markov process which have the same parameters as listed in Table 3. The simulated dataset is as long as the real DGPS positioning solutions at 1 Hz, containing the same number of data points. Since the white noise and the 1st order Gauss-Markov process are ergodic processes and the simulated error time series is sufficiently long, one sample of simulation is sufficient to reflect the error characteristics. The Allan variance analysis method is applied to analyze the simulated data, generating the Allan plot as shown in Fig. 5. Comparison of Figs. 5 and 4 shows that the two Allan curves are consistent in both shape and magnitude except for the ending part due to the uncertainty of Allan variance, which indicates the noise types and their coefficients identified from the Allan plots of the DGPS solutions at 1 Hz are credible.

Additionally, the PSD was applied to the same raw DGPS solutions at 1 Hz by using *Welch's* method. *Welch's* method is a modified periodogram spectral estimation method based on time averaging over short and modified periodograms (Welch 1967). Nevertheless, due to the density of the high-frequency data points in the log–log PSD plot, it might be difficult to identify the noise type through the PSD plots. Hence, the frequency *averaging technique* IEEE (2008b) was used to reduce the number of points in the PSD result and make the noise term identification easier.

Figure 6 shows the spectral characteristics of the DGPS solution of 1 Hz with a flat segment that can be identified in the low-frequency region. The figure shows an approximately linear decline for the intermediate segment to which a dashed straight line with slope of −1.62 can be fitted. Considering the interaction of different noise types, for example, multiple GM processes with different correlation times and the influence of the white noise part on the right-hand side, the value of the slope can be considered to be close to the theoretical value of −2. Therefore, 1st order Gauss-Markov process, that is, the flat portion plus the intermediate linear-decline portion, can be identified as the dominant noise term for low frequency below 0.02 Hz. The ending segment on the right of the PSD curve is close to a straight line with 0 slope, which means white noise can

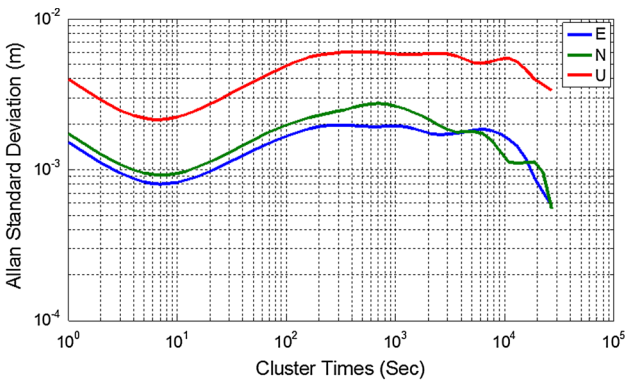

Fig. 5 Allan plots of the simulated dataset (to verify the analysis results)

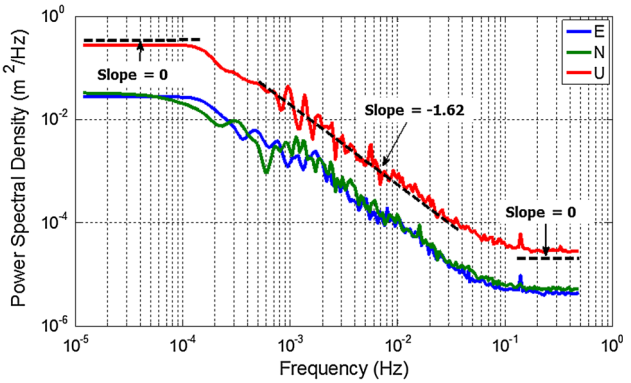

Fig. 6 Power spectral density functions of DGPS solution (1 Hz)

be identified in high-frequency span above 0.2 Hz. The comparison shows that the noise types identified by the Allan variance are consistent with that of PSD.

We analyzed six sets of DGPS positioning solutions at 1 Hz and 24 h each to investigate the repeatability of the Allan variance analysis results. The estimated coefficients for the white noise and the 1st Gauss-Markov process No. 1 (GM1) are listed in Tables 4 and 5, respectively. The tables indicate the estimated coefficients are close to each other for different sets of solutions, which means the error characteristics of the GNSS positioning solutions have good consistency. As a result, each of the individual solution can be used as a representation for the error characteristics analysis.

DGPS solution of 50 Hz

Figure 7 shows the time series of the positioning error of the DGPS solution at 50 Hz. It indicates that the post-processing DGPS can reach the precision of 6 mm and 15 mm (1 σ) in horizontal and vertical directions, respectively, which is roughly consistent with the accuracy of the DGPS solution at 1 Hz, that is, 4 and 10 mm. A log–log plot of Allan deviation versus the cluster time is shown in Fig. 8.

Table 4 Estimated coefficients of white noise for six sets of DGPS solutions (1 Hz)

Test no.	$E\ (mm/\sqrt{Hz})$	$N\ (mm/\sqrt{Hz})$	$U\ (mm/\sqrt{Hz})$
1	1.5	1.7	3.9
2	1.6	1.8	4.1
3	1.5	1.7	3.9
4	1.5	1.7	3.8
5	1.6	1.8	4.2
6	1.5	1.7	4.0
Mean	1.53	1.73	3.98
STD	0.05	0.05	0.15

Table 5 Estimated coefficients of GM1 for six sets of DGPS solutions (1 Hz)

Test no.	*E*		*N*		*U*	
	T_C (s)	σ_{GM} (mm)	T_C (s)	σ_{GM} (mm)	T_C (s)	σ_{GM} (mm)
1	124.7	2.8	130.5	3.3	175.4	7.7
2	120.3	2.7	132.4	3.5	170.1	7.4
3	124.7	2.7	133.7	3.0	167.4	6.9
4	124.7	2.8	128.4	3.2	172.2	7.0
5	124.7	2.7	135.7	3.3	171.8	7.6
6	124.7	2.8	131.4	3.2	175.4	7.6
Mean	124.0	2.8	132.0	3.3	172.1	7.4
STD	1.8	0.05	2.5	0.16	3.1	0.34

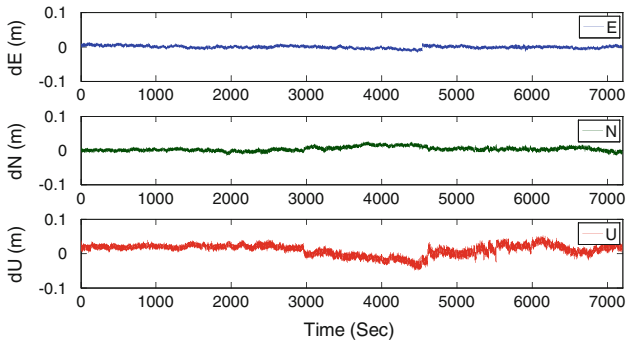

Fig. 7 Positioning error of DGPS solution (50 Hz)

Figure 8 shows that an apparent local maximum can be identified for the cluster time $T < 1$ s, which means time-correlated noise is the dominant term in this region rather than the white noise. This seems inconsistent with the conclusion of the DGPS solutions at 1 Hz, but it is reasonable. As mentioned above, receiver measurement noise and remaining tropospheric delay are the dominant error sources for the short-length baseline DGPS solution. This high-frequency time-correlated noise is most likely induced by the receiver, namely measurement noise. The GPS receiver is indeed capable of providing observations without any time-correlated noise at a relatively low sampling rate, for example, <1 Hz; but the noise is no long independent between consecutive observables at high sampling rate, for example, >1 Hz (Borre and Tiberius 2000). This time-correlated noise essentially reflects the low-pass effect of the carrier phase tracking loop inside the Trimble receiver. The right-hand side of the local maximum seems steeper than −1/2, which may be related to the higher order, that is, second or third order, of the loop filter (Xie 2009). In our research, this type of correlated noise was approximately modeled as 1st order Gauss-Markov process to keep the modeling concise.

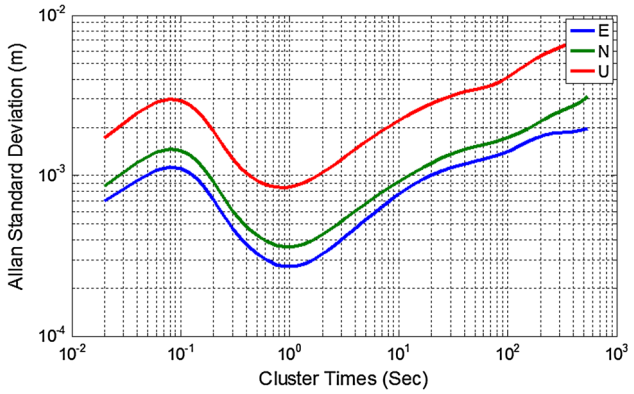

Fig. 8 Allan plots of DGPS solution (50 Hz)

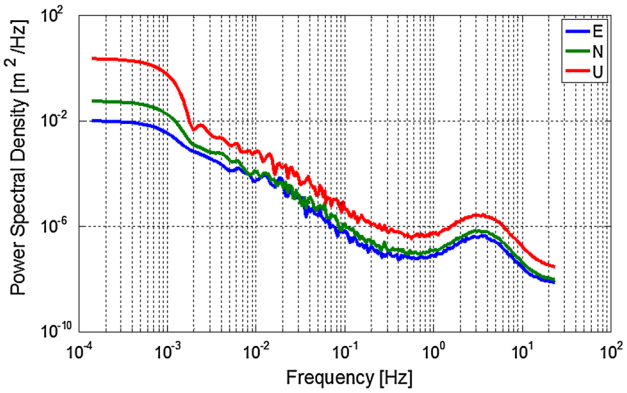

Fig. 9 Power spectral density functions of DGPS solution (50 Hz)

For cluster time $T > 2$ s, the Allan plot shows an approximately linear increase with a slope of 0.46, close to +1/2, which means random walk is the dominant noise term in large cluster time region. This random walk noise can be regarded as the left-hand part of the 1st order Gauss-Markov process in Fig. 4. The detailed explanation will be given in the next section. The coefficients of noises identified in DGPS solutions at 50 Hz are listed in Table 6.

The PSD analysis was also applied to the DGPS solutions of 50 Hz to validate the Allan variance analysis as shown in Fig. 9. At low-frequencies region, the PSD plot is close to a straight line with slope of −2, which means random walk is the dominant noise. An local maxima can be identified in the high-frequency region above 1 Hz, which means the output of the system exhibits the characteristics of high order, for example, second or third order, time-correlated noise. This is caused by the equivalent low-pass filter function for the carrier phase tracking with high order, as mentioned before. The result indicates the noise types identified by the PSD and the Allan variance methods are same.

Comparison of DGPS of 1 and 50 Hz

A comparison of the Allan plots of DGPS solution at 1 Hz shown in Fig. 4 and 50 Hz shown in Fig. 8 indicates the two figures are consistent with each other in both shape and the magnitude for the overlap part of the cluster time, for example, 10–200 s. For the cluster time T < 10 s, the white noise identified in Fig. 4 is actually the right-hand part of the 1st order Gauss-Markov process identified at the short cluster portion, that is, cluster time $T < 1$ s, of Fig. 8. However, they are different in magnitude, such as the value of white noise part for DGPS solution of 1 Hz is higher than that of 50 Hz. This is because the 1 Hz sampling rate is actually under-sampling for the GNSS receiver whose equivalent sensing bandwidth is around 20 Hz. Such under-sampling resulted in the higher noise magnitude in the Allan plot. Similarly, the random walk identified in Fig. 8 is actually the left-hand part of the 1st order Gauss-Markov process identified in Fig. 4. Different from the noise part, the magnitudes kept consistent very well, which is because the under-sampling issue does not exist for the long-term errors. Due to the large uncertainty of the ending part of Fig. 8, the region when cluster time $T > 200$ s will not be discussed.

Table 6 Noises identified in DGPS solutions (50 Hz)

Direction	GM		Random walk
	T_C (s)	σ_{GM} (mm)	$K\,(\mathrm{mm}/\sqrt{s})$
E	0.042	1.8	0.42 ± 0.01
N	0.042	2.4	0.51 ± 0.01
U	0.042	4.9	1.23 ± 0.03

Theoretically, white noise and random walk can be regarded as two limits of the 1st order Gauss-Markov process. When cluster time $T \ll T_C$, the 1st order Gauss-Markov process can be regarded as random walk noise, while for $T \gg T_C$, it can be regarded as white noise. So if the DGPS solution at 50 Hz could be long enough, for example, 24 h, then we would be able to observe the whole raised pattern representing the 1st order Gauss-Markov process. So based on the analysis above, we can conclude that the random walk noise is most likely induced by the remaining tropospheric delay as it is for the DGPS solutions at 1 Hz.

It should be noted here that the analysis of DGPS solutions at 1 and 50 Hz are based on short-length baseline. The error components in DGPS positioning solutions might change as the length of the baseline increases, for example tens of kilometers.

Allan variance analysis to PPP Solution

The Allan analysis will be applied to PPP positioning solutions at 1 and 50 Hz. The result will be presented

directly without detailed discussion, since the analysis procedure is similar to that of DGPS.

PPP solution of 1 Hz

The Allan plot of PPP positioning solutions at 1 Hz is shown as Fig. 10. From this figure, flicker noise can be identified as the dominant noise term for cluster time $T < 1$ s and the dominant noise term for the intermediate segment, that is $1 < T < 1{,}000$ s, is the 1st order Gauss-Markov process. For the ending part, it is hard to identify the noise type due to the large uncertainty of the Allan variance. Table 7 lists the estimated coefficients of the flicker noise and the 1st order Gauss-Markov process.

PPP solution of 50 Hz

Figure 11 is the Allan plots of PPP positioning solution of 50 Hz, which shows that the dominant noise term can be approximately modeled as 1st order Gauss-Markov process for cluster time $T < 0.5$ s. The coefficients for this noise term are listed in Table 8. A comparison of the coefficients in Tables 6 and 8 shows that GM processes identified in the 50 Hz PPP and DGPS solutions have the same correlated time and similar magnitude, which indicates they are caused by the equivalent bandwidth of the carrier phase tracking loop of the receivers.

Random walk can be identified for cluster time above 0.5 s whose coefficients are listed in Table 8. The large cluster time region, for example, $T > 400$ s, of the plots will not be discussed, since the curves along three different directions are not consistent with each other, which is caused by the increase of the estimation uncertainty of the Allan variances.

Allan variance analysis to SPP solution

The Allan variance analysis method is applied to SPP solutions at 1 Hz and 50 Hz. Since the analysis strategy is similar to that used above, the result will be presented directly with only brief explanations.

SPP solution of 1 Hz

The Allan plot of SPP positioning solution at 1 Hz, that is, Figure 12, shows an approximately linear decline at the beginning segment for cluster time $T < 10$ s. A straight line with a slope of -0.39, close to $-1/2$, can be fitted to this portion, which means white noise is the dominant noise term. The dominant noise can be modeled as 1st order Gauss-Markov process for large cluster time region, for example, $T > 500$ s, but for which the estimated coefficients may have large estimation uncertainty. For cluster time $10 < T < 400$ s, the plot looks like 1st order Gauss-Markov process. But due to the interactions of the other two noise terms identified above, part of the raised pattern representing the 1st Gauss-Markov process is masked. This speculation can be validated in the analysis of SPP

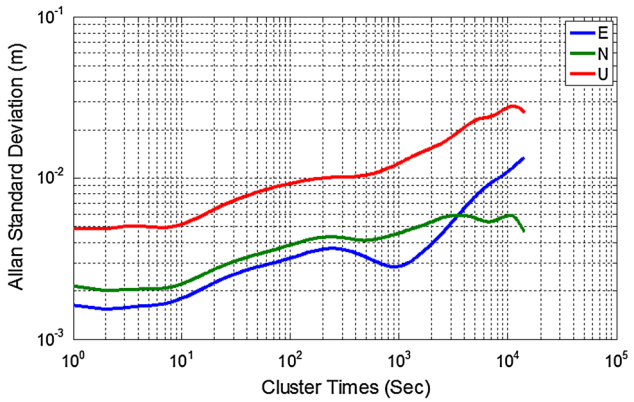

Fig. 10 Allan plots of PPP solution (1 Hz)

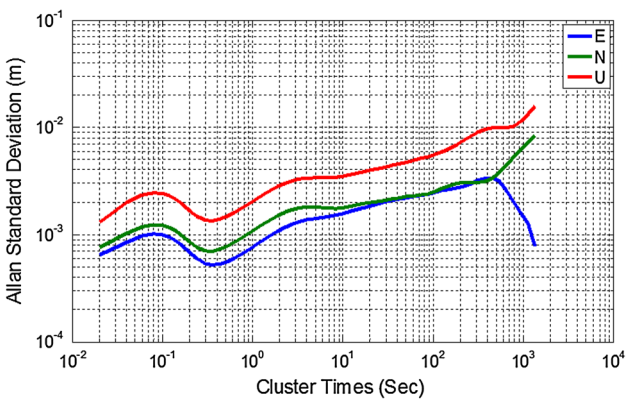

Fig. 11 Allan plots of PPP solution (50 Hz)

Table 7 Noises identified in PPP solutions (1 Hz)

Direction	Flicker noise	GM	
	B (mm)	T_C (s)	σ_{GM} (mm)
E	1.5	130.5	6.0
N	2.0	130.5	7.0
U	4.9	130.5	16.4

Table 8 Noises identified in PPP solution (50 Hz)

Direction	GM		Random walk
	T_C (s)	σ_{GM} (mm)	$K(\text{mm}/\sqrt{s})$
E	0.042	1.6	1.6
N	0.042	2.0	2.2
U	0.042	4.0	4.2

solutions at 50 Hz later. Table 9 lists the estimated coefficients of noise identified in SPP solutions of 1 Hz.

SPP solution of 50 Hz

The Allan plot of SPP solution of 50 Hz in Fig. 13 shows that two raised regions can be identified and a straight line with a slope of 0.41 can be fitted to the beginning segment of the plot. Considering the interaction of different noises, the dominant term for SPP solution at 50 Hz can be modeled as superposition of the two 1st order Gauss-Markov processes with different correlation times. Table 10 lists their estimated coefficients.

A comparison of Figs. 12 and 13 indicates that the noise suspected to be 1st order Gauss-Markov process at the cluster time of $10 < T < 400$ s in Fig. 12 can be confirmed in Fig. 13.

Conclusion

We made an attempt to characterize the GNSS positioning errors by using the Allan variance analysis method. Time series of GPS positioning error in three different modes, that is, DGPS, PPP, and SPP, are analyzed. Four dominant terms are identified in the GPS positioning solutions, that is, 1st order Gauss-Markov process, white noise, random walk noise, and flicker noise, which indicates that the GNSS positioning error components are complex. Consequently, it is not always optimal to model the GNSS positioning noise as white noise.

Allan variance analysis is proven to be an effective and feasible method to analyze the characteristics of the GNSS positioning error and build precise error models.

The models can be used for investigating the GNSS error sources, which is important for the improving the GNSS positioning techniques. Meanwhile, the precise GNSS positioning error models can be used in the GNSS/INS integration algorithms to optimize the navigation results, for example, make the variance of the estimation match the actual error level. Therefore, the Allan variance analysis method can be proposed for the GNSS positioning research and evaluation in the future, with some conventional method, for example, PSD as supplement if necessary.

As future work, the characteristics positioning error of long baseline DGPS solution and BeiDou Navigation Satellite System (BDS) are to be investigated using the Allan variance analysis method.

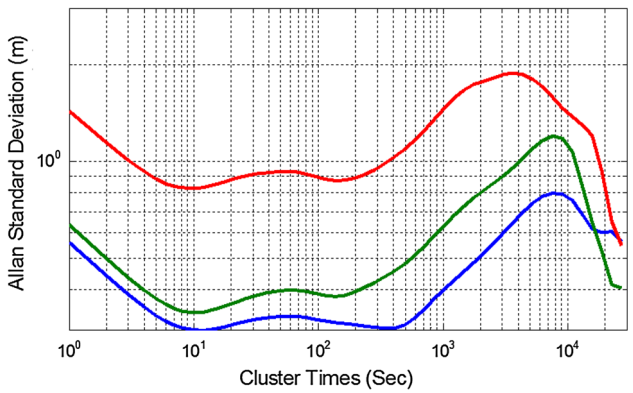

Fig. 12 Allan plots of SPP solution (1 Hz)

Table 9 Noises identified in SPP solution (1 Hz)

Direction	GM1		GM2		White noise
	T_C (s)	σ_{GM} (mm)	T_C (s)	σ_{GM} (mm)	$N\,(m/\sqrt{Hz})$
E	29.1	0.29	4,150	1.68	0.56
N	29.1	0.41	4,150	3.80	0.64
U	29.1	2.29	2,780	8.54	1.44

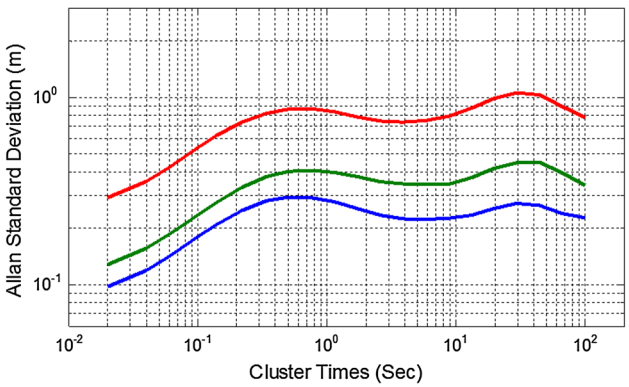

Fig. 13 Allan plots of SPP solution (50 Hz)

Table 10 Estimated coefficients for 1st order Gauss-Markov process for SPP solution (50 Hz)

Direction	GM1		GM2	
	T_C (s)	σ_{GM} (mm)	T_C (s)	σ_{GM} (mm)
E	0.402	0.47	15.608	0.44
N	0.402	0.66	15.608	0.72
U	0.402	1.41	15.608	1.71

References

Amiri-Simkooei AR, Tiberius CCJM, Teunissen PJG (2007) Assessment of noise in GPS coordinate time series: methodology and results. JGR 112:B07413. doi:10.1029/2006JB004913

Bierman GS (1995) Error modeling for differential GPS. Master thesis Charles Stark Draper Laboratory Inc., National Aeronautics and Space Administration, National Technical Information Service

Bock Y, Nikolaidis RM, de Jonge PJ, Bevis M (2000) Instantaneous geodetic positioning at medium distances with the Global Positioning System. JGR 105 (B12): 28,223–28,253, doi: 10.1029/2000JB900268

Borre K, Tiberius CCJM (2000) Time series analysis of GPS observables. Proc.ION-GPS-2000, Salt Lake city, Utah, pp 1885–1894

EI-Sheimy N, Hou HY, Niu XJ (2008) Analysis and modeling of inertial sensors using Allan variance. IEEE Trans Instrum Meas 57(1):140–149

El-Rabbany A, Kleusberg A (2003) Effect of temporal physical correlation on accuracy estimation in GPS relative positioning. Journal of Surveying Engineering 129(1):28–32. doi:10.1061/(ASCE)0733-9453

Feissel-Vernier M, De Viron O, Le Bail K (2007) Stability of VLBI, SLR, DORIS, and GPS positioning. Earth Planets Space 59(6):475–497

Friederichs T (2010) Analysis of geodetic time series using Allan variance. An investigation based on a coursework, University of Stuttgart. [Online]

Ge MR, Liu JN (1996) The estimation methods for tropospheric delays in global positioning system (in Chinese). Acta Geodaetica et Cartographica Sinica 25(4):285–291

Genrich JF, Bock Y (2006) Instantaneous geodetic positioning with 10–50 Hz GPS measurements: noise characteristics and implications for monitoring networks. JGR 111:B03403. doi:10.1029/2005JB003617

Groves PD (2008) Principles of GNSS, inertial and multisensor integrated navigation systems. Artech House

Hackl M, Malservisi R, Hugentobler U, Wonnacott R (2011) Estimation of velocity uncertainties from GPS time series: Examples from the analysis of the South African TrigNet network. JGR 116(B15): B11404. doi: 10.1029/2010JB008142

Howind J, Kutterer H, Heck B (1999) Impact of temporal correlations on GPS-derived relative point positions. J Geodesy 73:246–258

IEEE (2008a) Standard Specification Format Guide and Test Procedure for Linear, Single-Axis, Non-gyroscopic Accelerometers, IEEE Std. 1293–1988, pp 166–182

IEEE (2008b) Standard specification format guide and test procedure for single-axis interferometric fiber optic gyros, IEEE Std. 952–1997 (R2008), pp 61–73

Khelifa S, Kahlouche S, Belbachir MF (2011) Noise characteristics of GPS coordinate time series. International Journal of Academic Research. 3(3), II Part: 589–596

King NE, Svarc JL, Fogleman EB, Gross WK, Clark KW, Hamilton GD, Stiffler CH, Sutton JM (1995) Continuous GPS observations across the Hayward fault, California, 1991–1994. JGR 100(B10): 20,271–20,283. doi:10.1029/95 JB02035

Land DV, Levick AP, Hand JW (2007) The use of the Allan deviation for the measurement of the noise and drift performance of microwave radiometers. Meas Sci Technol 18:1917–1928

Langbein J, Johnson H (1997) Correlated errors in geodetic time series: implications for time dependent deformation. JGR 102(B1):591–603. doi:10.1029/96JB02945

Liu JN, Ge (2003) PANDA software and its preliminary result of positioning and orbit determination. Wuhan University Journal of Natural Sciences 8(B2):603–609. doi:10.1007/BF02899825

Malkin ZM (2011) Study of astronomical and geodetic series using the Allan variance. Kinematics Phys Celestial Bodies 27(1):42–49

Mao A, Harrison CGA, Dixon TH (1999) Noise in GPS coordinate time series. JGR 104(B2):2797–2816. doi:10.1029/1998JB900033

Niu XJ, Zhang Q, Zhang HP (2010) Use Allan Variance to Analyze the Results of GNSS/INS Navigation Systems. Proceedings of the CPGPS 2010 Technical Forum on Satellite Navigation and Positioning, Shanghai, China. pp 565–572

Rankin J (1994) An error model for sensor simulation GPS and differential GPS. IEEE Position Location and Navigation Symposium Record: pp 260–266

Riley WJ (2008) Handbook of frequency stability analysis. US Department of Commerce, National Institute of Standards and Technology

Roberts CA, Morgan P, Rizos C (2002) Allan variance applied to time series baseline results for GPS-based deformation monitoring applications. Proceedings of the 2nd symposium on geodesy for geotechnical and structural applications, Berlin: pp 99–311

Shin EH (2001) Accuracy improvement of low cost INS/GPS for land applications. Master thesis, University of Calgary, Alberta, pp 29–46

Tralli DM, Lichten SM (1990) Stochastic estimation of tropospheric path delays in Global Positioning System geodetic measurements. J Geodesy 64(2):127–159

Welch PD (1967) The use of fast fourier transform for the estimation of power spectra: a method based on time averaging over short, modified periodograms. IEEE Trans on 15:70–73

Williams SDP, Bock Y, Fang P, Jamason P, Nikolaidis RM, Prawirodirdjo L, Miller M, Johnson DJ (2004) Error analysis of continuous GPS position time series. JGR 109(B3):B3412. doi:10.1029/2003JB002741

Xie G (2009) Principles of GPS and receiver design. Publishing House of Electronics Industry, Beijing, pp 266–303

Zhang J, Bock Y, Johnson H, Fang P, Genrich JF, Williams S, Wdowinski S, Behr J (1997) Southern California permanent GPS geodetic array: error analysis of daily position estimates and site velocities. JGR 102(B8):18,035–18055. doi:10.1029/97JB01380

Author Biographies

Xiaoji Niu received the B.Eng. degree (with honors) in mechanical and electrical engineering and the Ph.D. degree from Tsinghua University, Beijing, China, in 1997 and 2002, respectively. From 2003 to 2007, he was a Post Doctoral Fellow with the Mobile Multi-Sensor Systems (MMSS) Research Group, Department of Geomatics Engineering, University of Calgary. From 2007 to 2009, he was a Senior Scientist with SiRF Technology, Inc. He is currently a Professor of GNSS Research Center, Wuhan University. His research interests focus on INS and GNSS/INS integration.

Qijin Chen is a master student at Wuhan University. He obtained his Bachelor Degree from the School of Geodesy and Geomatics of Wuhan University. His current research mainly focuses on GNSS/INS integration algorithm and applications.

Quan Zhang is a Ph.D. candidate of GNSS Research Center at Wuhan University. He received the B.S. degree in Geomatics Engineering from Shandong University of Science and Technology in 2009. His research interest focuses on the inertial navigation and the GPS/INS integration technology.

Hongping Zhang is an associate professor in Wuhan University, China. Dr. Zhang received his doctorate degree in GNSS precise data processing and application in 2006. His main research interests include GNSS/ionosphere inversion research and GNSS/INS coupling. He has published about 20 papers on GNSS technologies and held/attended ten projects on GNSS data processing and application.

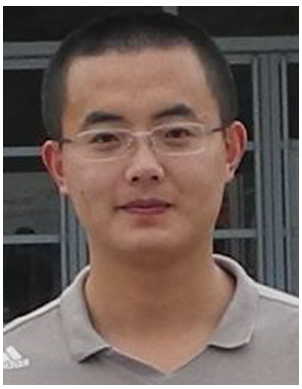

Jieming Niu received B.Sc degree in geomatics from Wuhan University in 2011 and currently works as a graduate student at Wuhan University. His main interests are high-rate GPS, accelerometer and its application on seismology and tsunami warning.

Kejie Chen is a postgraduate student of the GNSS Research Center of Wuhan University. He received his bachelor's degree in Chang'an University in 2010. The focus of his current research lies in precise GNSS data processing and its geologic application.

Chuang Shi is the head of GNSS Research Center of Wuhan University. He graduated from Wuhan University and obtained his PhD degree in 1998. His research interests include network adjustment, precise orbit determination of GNSS satellites and LEOs, and real-time precise point positioning (PPP).

Jingnan Liu is a member of Chinese Academy of Engineering, professor at Wuhan University, expert in geodesy and surveying engineering with the specialty of GNSS technology and applications. He has been the head of the National Engineering Research Center for Satellite Positioning System since 1998. He is currently an executive member of the council, Chinese Society for Geodesy Photogrammetry and Cartography, the editorial board member of GPS World, and the coordinator of the International GPS Geodynamics Services. He has published more than 150 academic papers and supervised more than 100 postgraduates.